



Magnetic Flux and Magnetic Nonpotentiality of Active Regions in Eruptive and Confined Solar Flares

Ting Li^{1,2}, Anqin Chen³, Yijun Hou^{1,2}, Astrid M. Veronig⁴, Shuhong Yang^{1,2}, and Jun Zhang⁵

¹ CAS Key Laboratory of Solar Activity, National Astronomical Observatories, Chinese Academy of Sciences, Beijing 100101, People's Republic of China; liting@nao.cas.cn

² School of Astronomy and Space Science, University of Chinese Academy of Sciences, Beijing 100049, People's Republic of China

³ Key Laboratory of Space Weather, National Center for Space Weather, China Meteorological Administration, Beijing 100081, People's Republic of China

⁴ Institute of Physics & Kanzelhöhe Observatory for Solar and Environmental Research, University of Graz, A-8010 Graz, Austria

⁵ School of Physics and Materials Science, Anhui University, Hefei 230601, People's Republic of China

Received 2021 July 5; revised 2021 August 2; accepted 2021 August 2; published 2021 August 20

Abstract

With the aim of understanding how the magnetic properties of active regions (ARs) control the eruptive character of solar flares, we analyze 719 flares of Geostationary Operational Environmental Satellite (GOES) class $\geq C5.0$ during 2010–2019. We carry out the first statistical study that investigates the flare–coronal mass ejection (CME) association rate as a function of the flare intensity and the AR characteristics that produce the flare, in terms of its total unsigned magnetic flux (Φ_{AR}). Our results show that the slope of the flare–CME association rate with flare intensity reveals a steep monotonic decrease with Φ_{AR} . This means that flares of the same GOES class but originating from an AR of larger Φ_{AR} , are much more likely to be confined. Based on an AR flux as high as 1.0×10^{24} Mx for solar-type stars, we estimate that the CME association rate in X100-class “superflares” is no more than 50%. For a sample of 132 flares $\geq M2.0$ class, we measure three nonpotential parameters including the length of steep gradient polarity-inversion line (L_{SGPIL}), the total photospheric free magnetic energy (E_{free}), and the area with large shear angle (A_{Ψ}). We find that confined flares tend to have larger values of L_{SGPIL} , E_{free} , and A_{Ψ} compared to eruptive flares. Each nonpotential parameter shows a moderate positive correlation with Φ_{AR} . Our results imply that Φ_{AR} is a decisive quantity describing the eruptive character of a flare, as it provides a global parameter relating to the strength of the background field confinement.

Unified Astronomy Thesaurus concepts: [Solar activity \(1475\)](#); [Solar active region magnetic fields \(1975\)](#); [Solar flares \(1496\)](#); [Solar coronal mass ejections \(310\)](#); [Stellar activity \(1580\)](#)

1. Introduction

Solar flares and coronal mass ejections (CMEs) are the most catastrophic phenomena in the present solar system, driven by a sudden release of magnetic energy stored in the solar corona. Large solar flares are often, but not always, associated with CMEs. We dub flares with a CME as “eruptive” and flares without a CME as “confined” (Moore et al. 2001). There are two main factors that are considered to determine whether or not a flare event is CME-eruptive. One factor is the constraining effect of the background magnetic field overlying the flaring region, i.e., the strength of magnetic field or its decay with height (Wang & Zhang 2007; Yang et al. 2014; Thalmann et al. 2015; Baumgartner et al. 2018). Li et al. (2020) analyzed 322 large flares and found that the flare–CME association rate decreases with the increasing magnetic flux of the active region (AR) that produces the flare, implying that large magnetic flux generally tends to confine eruptions.

Another factor determining the eruptive character of solar flares is thought to be related to magnetic complexity and nonpotentiality of ARs (Sun et al. 2015; Liu et al. 2016; Jing et al. 2018; Duan et al. 2019), such as free magnetic energy, relative helicity, magnetic twists, etc. Numerous statistical studies have revealed that strong flares mostly occur in ARs with a complex configuration and high nonpotentiality of magnetic fields (Mayfield & Lawrence 1985; Falconer et al. 2002; Chen & Wang 2012, 2020; Su et al. 2014). However, there are only a few statistical studies focusing on magnetic nonpotential measures in confined versus eruptive flares (Nindos & Andrews 2004; Cui et al. 2018; Vasantharaju

et al. 2018). Nindos & Andrews (2004) and Gupta et al. (2021) found that in a statistical sense the pre-flare coronal magnetic helicity of ARs producing confined large flares is smaller than that of ARs producing eruptive large flares. Bobra & Ilonidis (2016) used machine-learning algorithms to predict CME productivity and found that the “intensive” parameters (those not scaling with the AR size) distinguish between eruptive and confined flares. Until now, the key nonpotential parameters of ARs governing the eruptive character of solar flares are still unknown based on statistical results. Moreover, the access to open flux (open to the interplanetary space) is also thought to influence whether an X-class flare is likely to be eruptive (DeRosa & Barnes 2018).

In this Letter, we carry out the first statistical study that investigates the flare–CME association rate R as a function of the AR characteristics that produce the flare, in terms of its total magnetic flux (Φ_{AR}). Our findings reveal clear differences of R , with the slope of R as a function of flare intensity being a monotonically decreasing function of Φ_{AR} . This result has important implications for the prediction of CMEs occurring in association with large flares as well as for the solar–stellar connection, where the solar flare–CME association rates are used to estimate stellar CME occurrence frequencies. Moreover, we also find the distinct differences of nonpotential parameters characterizing ARs in eruptive and confined large flares.

Table 1Number of Eruptive and Confined Flares in all ARs and ARs with Largest Φ_{AR}

Class	Eruptive ^a	Confined ^a	R^b	Eruptive ^c	Confined ^c	R^b
C	82	315	21%	1	40	2%
M	154	147	51%	6	30	17%
X	15	6	71%	1	4	20%
Total	251	468	35%	8	74	10%

Notes.^a For all ARs.^b Flare–CME association rate.^c For ARs with the largest $\Phi_{\text{AR}} > 9.0 \times 10^{22}$ Mx.**2. Observational Data and Analysis***2.1. Data and Event Selection*

We check for the soft X-ray (SXR) flare catalog recorded by the Geostationary Operational Environmental Satellite (GOES) system and select flare events $\geq C5.0$ occurring within 45° from the central meridian, from 2010 to 2019 June. A total of 719 events are selected, including 322 M-class (Li et al. 2020) and 397 C-class flares. To determine whether a flare is associated with a CME, we use the CME catalog⁶ of the Solar and Heliospheric Observatory/Large Angle and Spectrometric Coronagraph (Brueckner et al. 1995). The observations from the Atmospheric Imaging Assembly (AIA; Lemen et al. 2012) on board the Solar Dynamics Observatory (SDO; Pesnell et al. 2012) and the twin Solar Terrestrial Relations Observatory (Howard et al. 2008; Kaiser et al. 2008) are also used to help determining the CME association (see the detailed description in Li et al. 2020). Out of these 719 flares, 251 events are eruptive and 468 are confined (see Table 1 and the database FlareC5.0⁷). For each event, we calculated Φ_{AR} before the flare onset (within 30 min) by using the available vector magnetograms from Space-Weather Helioseismic and Magnetic Imager (HMI; Scherrer et al. 2012) AR Patches (SHARP; Bobra et al. 2014). Only pixels that host a radial component of the magnetic field $|B_r| > 100$ G are considered (Kazachenko et al. 2017).

2.2. Calculation of Magnetic Nonpotential Parameters of ARs

For a subset of 132 flare events $\geq M2.0$ (86 eruptive and 46 confined), we calculated three nonpotential parameters before the flare onset (within 30 minutes) including the length of polarity-inversion lines (PILs) with steep horizontal magnetic gradient (L_{SGPIL}), the total photospheric free magnetic energy (E_{free}) and the area with strong magnetic shear (A_Ψ). Magnetic PILs mark the separation between positive and negative magnetic flux in the photosphere of ARs. Properties of PILs in ARs have been found to be strongly correlated to solar flare and CME occurrences (Falconer et al. 2002; Vasantharaju et al. 2018; Kontogiannis et al. 2019; Wang et al. 2020). High-gradient, strong-field PILs are proxies of (near-)photospheric compact electrical currents and the occurrence of major flares was often associated with the emergence of flux with high-gradient, strong-field PILs (Schrijver 2007; Toriumi & Wang 2019). According to the method of Chen & Wang (2012), we measured the length of the PILs with a steep

horizontal magnetic gradient (≥ 300 G Mm⁻¹) for each flare event based on the SHARP vector magnetograms.

The energy that is released during a flare is generally believed to originate from the free magnetic energy stored primarily in ARs, which is the amount of magnetic energy in excess of the minimum energy attributed to the potential field (Molodensky 1974). It was found that the higher the free magnetic energy stored in an AR, the larger the size (magnitude) of upcoming flares (Jing et al. 2010; Su et al. 2014). We use a proxy for the total photospheric free magnetic energy (Wang et al. 1996; Chen & Wang 2012), which can be calculated as

$$E_{\text{free}} = \Sigma \rho_{\text{free}} dA, \quad (1)$$

where ρ_{free} is a proxy for the density of the free magnetic energy in the photosphere, defined as

$$\rho_{\text{free}} = \frac{|\mathbf{B}_o - \mathbf{B}_p|^2}{8\pi}, \quad (2)$$

where \mathbf{B}_o and \mathbf{B}_p are the observed and the potential magnetic fields, respectively. \mathbf{B}_p was derived from the observed B_r component using the Fourier transform method. ρ_{free} and E_{free} are in units of (erg cm⁻³) and (erg cm⁻¹), respectively. We measured E_{free} by only considering the pixels with $\rho_{\text{free}} \geq 4.0 \times 10^4$ erg cm⁻³.

Magnetic shear, defined as the angular difference between the measured field and the calculated potential field, is another commonly used parameter in describing the magnetic complexity and nonpotentiality (Wang et al. 1994; Zhang et al. 2007). We measured the area with shear angle $\geq 80^\circ$, A_Ψ (Chen & Wang 2012). The shear angle is given by

$$\Psi = \arccos \frac{\mathbf{B}_o \cdot \mathbf{B}_p}{|B_o B_p|}. \quad (3)$$

3. Statistical Results*3.1. Relations of Flare–CME Association Rate with Flare Intensity and Magnetic Flux of ARs*

We investigate the flare–CME association rate R as function of both the flare class and the total flux of the source AR for 719 flares ($\geq C5.0$ class). Figure 1(a) shows the scatter plot of Φ_{AR} versus flare peak SXR flux (F_{SXR}). Blue (red) circles are the eruptive (confined) flares. Obviously, when Φ_{AR} is large enough ($> 1.0 \times 10^{23}$ Mx; black dashed line), an overwhelming majority (about 97%) of flares do not generate CMEs (57 of 59 flares are confined). Out of the flare events of $\Phi_{\text{AR}} > 1.0 \times 10^{23}$ Mx (a total of 59 events), 32 flares occurred in AR 12192, the huge AR known as flare-rich but CME-poor (Sun et al. 2015), and the fraction is about 54%. If we remove the events in AR 12192, almost all the events are confined (26 of 27 flares are confined).

The value of Φ_{AR} for the 719 flares ranges from 8.5×10^{21} Mx to 2.3×10^{23} Mx, and we divide Φ_{AR} into five subintervals. Figure 1(b) shows the relations of the association rate R with F_{SXR} within the five Φ_{AR} subintervals. For each subinterval, R clearly increases with F_{SXR} . Each straight line in Figure 1(b) shows the linear fit

$$R = \alpha \log F_{\text{SXR}} + \beta, \quad (4)$$

⁶ https://cdaw.gsfc.nasa.gov/CME_list/⁷ <https://doi.org/doi:10.12149/101067>

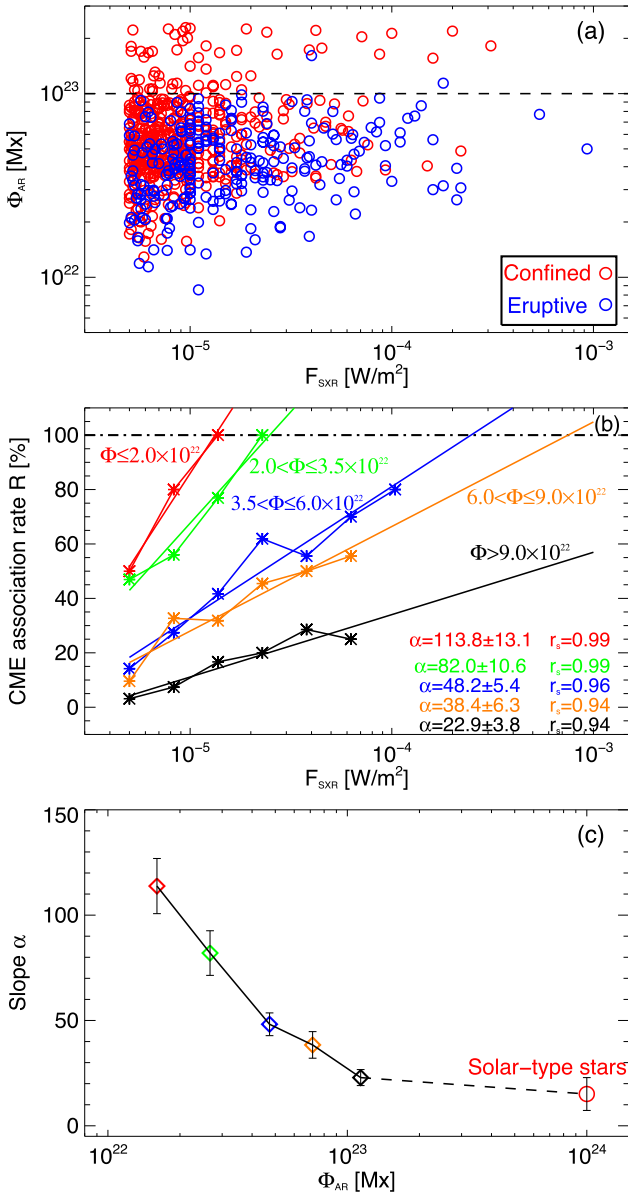


Figure 1. Relations of flare–CME association rate (R) with flare peak soft X-ray flux (F_{SXR}) and total unsigned magnetic flux of ARs (Φ_{AR}). (a) Scatter plots of Φ_{AR} vs. F_{SXR} . Blue (red) circles are the eruptive (confined) flares (\geq C5.0 class). Black dashed line corresponds to Φ_{AR} of 1.0×10^{23} Mx. (b) Association rate R as a function of F_{SXR} separately for five different subintervals of Φ_{AR} . The colored straight lines show the results of linear fitting, and slopes α and Spearman rank order correlation coefficients r_s are shown at the bottom right. (c) Plot of slope α vs. Φ_{AR} (plotted at the average of the log values in each subinterval). Colored diamonds denote the slopes α in five different Φ_{AR} subintervals. The red circle is the estimated value of slope α (about 15.1) for solar-type stars by assuming Φ_{AR} of 1.0×10^{24} Mx (Maehara et al. 2012; Shibata et al. 2013).

where R is in percentage and F_{SXR} is in units of W m^{-2} . For the smallest Φ_{AR} subinterval ($\leq 2.0 \times 10^{22}$ Mx), the slope α is 113.8 ± 13.1 and R reaches 100% when the flare is $>$ M1.3 class (red straight line). For the subinterval of $2.0 < \Phi_{\text{AR}} \leq 3.5 \times 10^{22}$ Mx, the slope α decreases to 82.0 ± 10.6 (green straight line). It can be seen that in ARs with a small Φ_{AR} , about 50% C5.0-class flares have associated CMEs. For the moderate Φ_{AR} subintervals (blue and orange lines), the slopes α are 48.2 ± 5.4 and 38.4 ± 6.3 , respectively.

The Spearman rank order correlation coefficients r_s are 0.96 and 0.94, respectively. In ARs with the largest Φ_{AR} ($> 9.0 \times 10^{22}$ Mx), R decreases significantly when compared to subintervals characterized by smaller Φ_{AR} (black straight line; also see Table 1). The relation between R and F_{SXR} in the largest Φ_{AR} subinterval is

$$R = (22.9 \pm 3.8) \log F_{\text{SXR}} + (125.7 \pm 17.9). \quad (5)$$

Based on Equation (5), only 20% of all M-class flares originating from the largest ARs have associated CMEs and the rate R reaches about 40% for flares $>$ X2. Almost all C5.0-class flares are confined due to the strong constraining fields in the largest ARs.

Figure 1(c) shows the relation of the slope α with Φ_{AR} . Φ_{AR} is defined here as the mean of the individual log values in each Φ_{AR} subinterval. The plot shows that the slope α decreases monotonically with increasing Φ_{AR} . We assume ARs in solar-type stars of $\Phi_{\text{AR}} \sim 1.0 \times 10^{24}$ Mx (Maehara et al. 2012; Shibata et al. 2013). Because there are only five known slope values, it is difficult to fit the plot and make an extrapolation. We use the slope in the largest solar ARs, i.e., 22.9, minus the average error estimate of five known slope values (~ 7.8 , corresponding to the average error of five diamonds), that is 22.9 minus 7.8 equals 15.1 as the slope α for stellar ARs of $\Phi_{\text{AR}} \sim 1.0 \times 10^{24}$ Mx. We estimate that the slope α might be no more than 15.1 ± 7.8 (red circle). If C5.0-class flares are all confined on solar-type stars (similar to the subinterval of $\Phi_{\text{AR}} > 9.0 \times 10^{22}$ Mx), we can extrapolate the flare–CME association rate for solar-type stars is given as

$$R = (15.1 \pm 7.8) \log F_{\text{SXR}} + 80.0. \quad (6)$$

Thus, for X100-class superflares in solar-type stars, the estimated association rate R is no more than 50%.

3.2. Magnetic Nonpotentiality of ARs in Eruptive and Confined Flares

We calculate three nonpotential parameters for 132 flares \geq M2.0. Figure 2 shows an example of an eruptive X2.2-class flare occurring on 2011 February 15 in AR NOAA 11158. The SG PIL is located between two flare ribbons, and the distributions of the photospheric free energy density ρ_{free} and shear angle Ψ show similar patterns. In Figure 3, we display the scatter plots and histograms of the three nonpotential measures for the whole set of 132 flare events. It can be seen that the distributions of L_{SGPIL} show evident differences between confined and eruptive cases (Figures 3(a)–(b)). For $L_{\text{SGPIL}} < 22$ Mm (black dashed–dotted line in Figure 3(a)), an overwhelming majority (about 90%) of flares are eruptive. The log-mean value of L_{SGPIL} for confined flares is 40.2 Mm (red dotted line in panel (b)), much larger than that for eruptive events (20.8 Mm, blue dotted line in panel (b)). The distributions of E_{free} are similar to those of L_{SGPIL} . For $E_{\text{free}} < 1.5 \times 10^{23}$ erg cm^{-1} (black dashed–dotted line in Figure 3(c)), 48 in 58 flares are eruptive. For $A_{\Psi} < 60$ Mm^2 , about 79% (30 in 38) flares are eruptive (Figure 3(e)). The log-mean values of E_{free} and A_{Ψ} for confined flares are much larger than those for eruptive events (Figures 3(d) and (f)).

In Figure 4, we investigate the relationship between the three nonpotential parameters and Φ_{AR} in Figure 4. It can be seen that each of the two nonpotential parameters have strong correlations at $r_s \sim 0.69$ – 0.85 (Figures 4(a)–(c)). The high

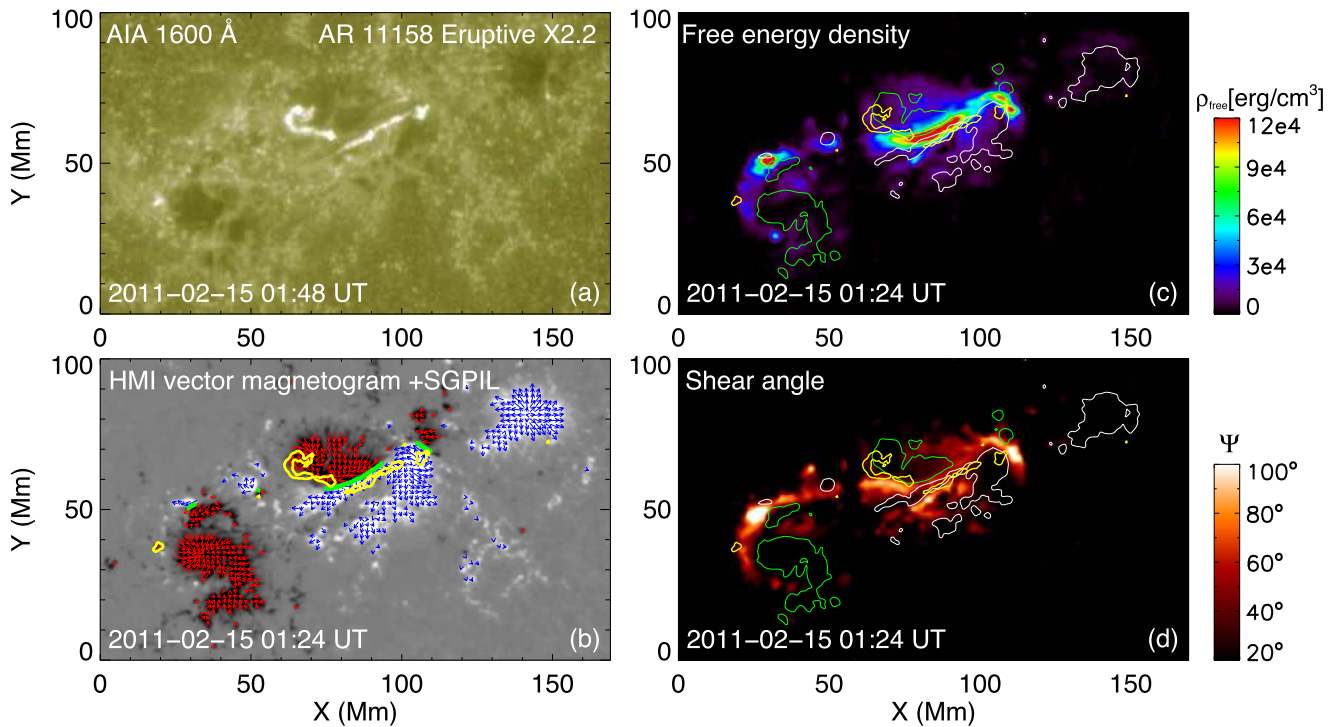


Figure 2. Tracing the magnetic polarity-inversion line with the steep horizontal magnetic gradient (SGPIL), photospheric free magnetic energy density ρ_{free} and the magnetic shear angle Ψ in AR 11158 on 2011 February 15. (a) SDO/AIA 1600 Å image showing the flare ribbon brightenings of an eruptive X2.2-class flare. (b) SDO/HMI vector magnetogram with horizontal magnetic field vectors (red and blue arrows) overlotted on the B_r map. SGPIL ($\geq 300 \text{ G Mm}^{-1}$) is shown as green lines. Yellow contours are the ribbon brightenings. (c) ρ_{free} distribution with contours of the B_r component and flare ribbon brightenings. The white (green) contours represent the positive (negative) polarity. (d) Ψ distribution with contours of the B_r component and ribbon brightenings.

correlation coefficients between L_{SGPIL} , E_{free} , and A_{Ψ} imply that ARs with long SGPIL tend to store more free magnetic energy and have strong shearing. The scatter plot of L_{SGPIL} with Φ_{AR} illustrates that they have a moderate correlation at $r_s \sim 0.4$ (Figure 4(d)). About 89% of the confined flares occur in ARs with $\Phi_{\text{AR}} > 3.5 \times 10^{22} \text{ Mx}$ and SGPIL longer than 22 Mm. Moderate correlations were also obtained for E_{free} versus Φ_{AR} and A_{Ψ} versus Φ_{AR} (Figures 4(e)–(f)). Their moderate correlations with Φ_{AR} indicate that there is some trend that the higher the magnetic flux of an AR, the higher the nonpotentiality of the AR.

4. Summary and Discussion

In this study, we have examined 719 flares $\geq \text{C5.0}$ class that were observed on-disk from 2010 to 2019 June. We investigate for the first time the flare–CME association rate R as a function of both the flare class F_{SXR} and the total flux Φ_{AR} of the AR that produces the flare. We find that, for each Φ_{AR} subinterval, R clearly increases with F_{SXR} , i.e., larger flares are more likely to be associated with a CME. This result is in agreement with previous findings studying CME–flare association rates (Andrews 2003; Yashiro et al. 2006), who reported overall CME associations of about 60% for M-class flares and 90% for X-class flares. However, what is new and particularly important in our study is that we considered not only the relation to the intensity of the flare but also to the characteristics of the AR in terms of its total magnetic flux. Our results show that the slope of the flare–CME association rate depends on the total flux of the AR that produces the flare, and reveals a steep monotonic decrease with Φ_{AR} (Figure 1(c)). This means that flares of the same GOES class but originating from an AR of larger Φ_{AR} ,

are much more likely confined. Within the smallest Φ_{AR} subinterval ($\leq 2.0 \times 10^{22} \text{ Mx}$), all flares $> \text{M1.3}$ are all eruptive. On the other end of the distribution for the largest Φ_{AR} subinterval ($> 9.0 \times 10^{22} \text{ Mx}$), only about 20% of M-class flares have associated CMEs and the association rate R reaches about 40% for those flares $> \text{X2}$.

Our results imply that Φ_{AR} is a key factor determining the eruptive character of solar flares, consistent with our previous studies (Li et al. 2020). Φ_{AR} can be considered to be both a measure of the total flux that is in principle available for flaring as well as being a measure of the background field confinement overlying the flaring region. Our findings imply that the latter is the more important factor here. Large Φ_{AR} means a strong confinement and thus the flare–CME association rate is relatively low compared to small Φ_{AR} . Moreover, based on solar observations, we can speculate the associate rate R on solar-type stars by assuming Φ_{AR} of $1.0 \times 10^{24} \text{ Mx}$ (Maehara et al. 2012; Shibata et al. 2013). For X100-class “superflares” on solar-type stars, no more than 50% of flares can generate stellar CMEs. This may provide an explanation of why the detection of stellar CMEs is rare (e.g., Leitzinger et al. 2014; Argiroffi et al. 2019; Moschou et al. 2019; Vida et al. 2019; Veronig et al. 2021), while extrapolating current flare–CME relations to solar-type stars leads to unphysically high CME rates (Drake et al. 2013; Odert et al. 2017). Our findings provide an important contribution to revise the flare–CME association rates for solar-type stars, by including the distinct differences in these relations in dependence of the AR magnetic flux.

Using HMI vector magnetograms, we also have studied the relation between the degree of magnetic nonpotentiality and the eruptive character of 132 flares $\geq \text{M2.0}$, finding distinct

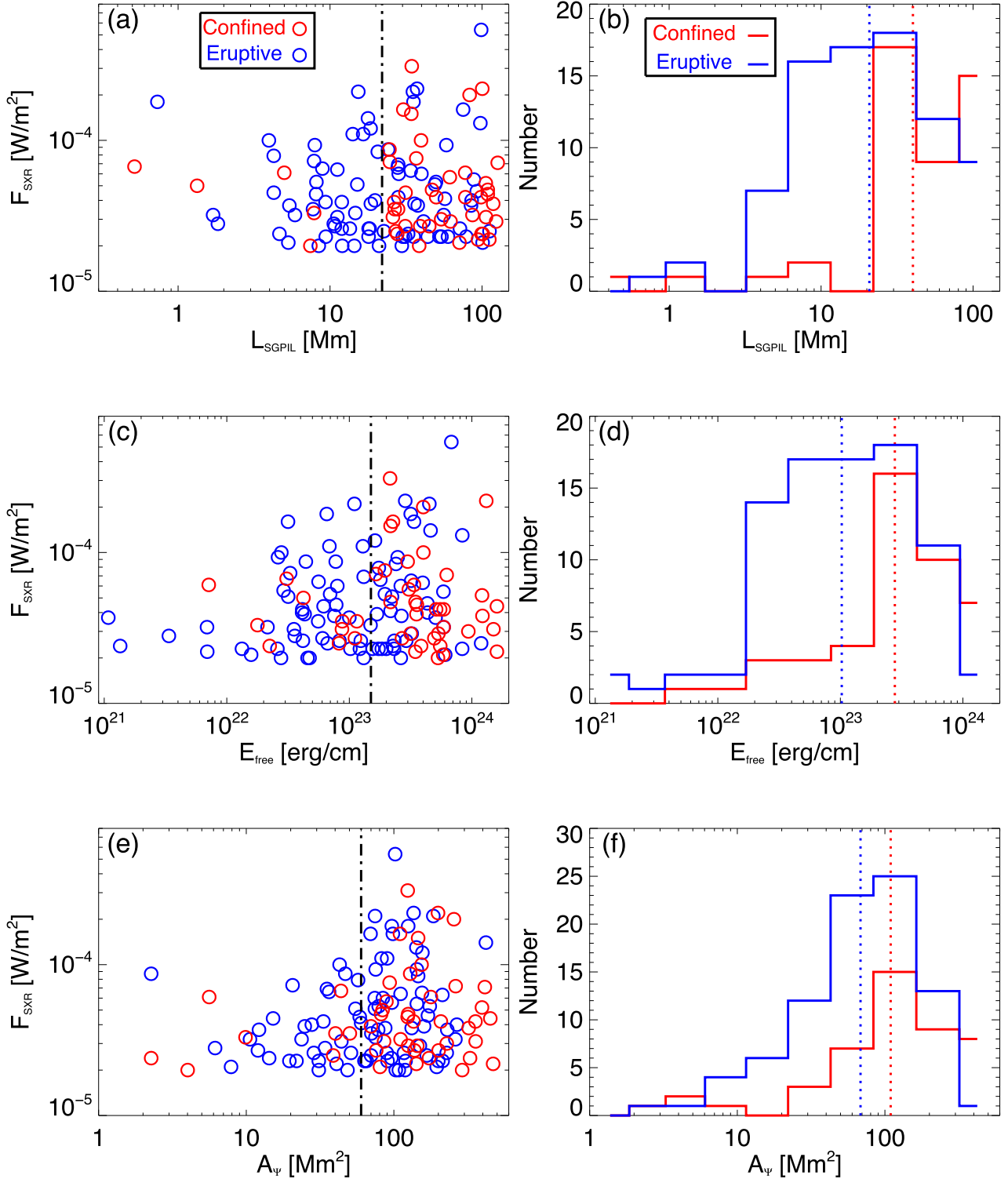


Figure 3. Scatter plots and histograms of three different nonpotentiality measures for eruptive (blue) and confined (red) flares ($\geq M2.0$ class). Top: scatter plot of F_{SXR} vs. SGPIL length (L_{SGPIL}) and the histogram of L_{SGPIL} . Black dashed-dotted line in panel (a) refers to L_{SGPIL} of 22 Mm. Dotted vertical lines in panel (b) indicate the means of the log values. Middle: scatter plot of F_{SXR} vs. the total free magnetic energy E_{free} and the histogram of E_{free} . Black dashed-dotted line in panel (c) refers to E_{free} of $1.5 \times 10^{23} \text{ erg cm}^{-1}$. Bottom: scatter plot of F_{SXR} vs. the area with strong magnetic shear A_{Ψ} and the histogram of A_{Ψ} . Black dashed-dotted line in panel (e) refers to A_{Ψ} of 60 Mm^2 .

differences between eruptive and confined flares for all three nonpotentiality parameters derived (Figures 3–4). L_{SGPIL} , E_{free} , and A_{Ψ} all give smaller log-mean values for eruptive flares than noneruptive flares. Each nonpotential parameter shows a

moderate correlation with Φ_{AR} . Our study shows that the three “extensive” parameters (those scaling with the AR size) can only discriminate the flares with small nonpotential parameters. As seen in Figure 3, 42 out of 47 events with $L_{\text{SGPIL}} < 22 \text{ Mm}$

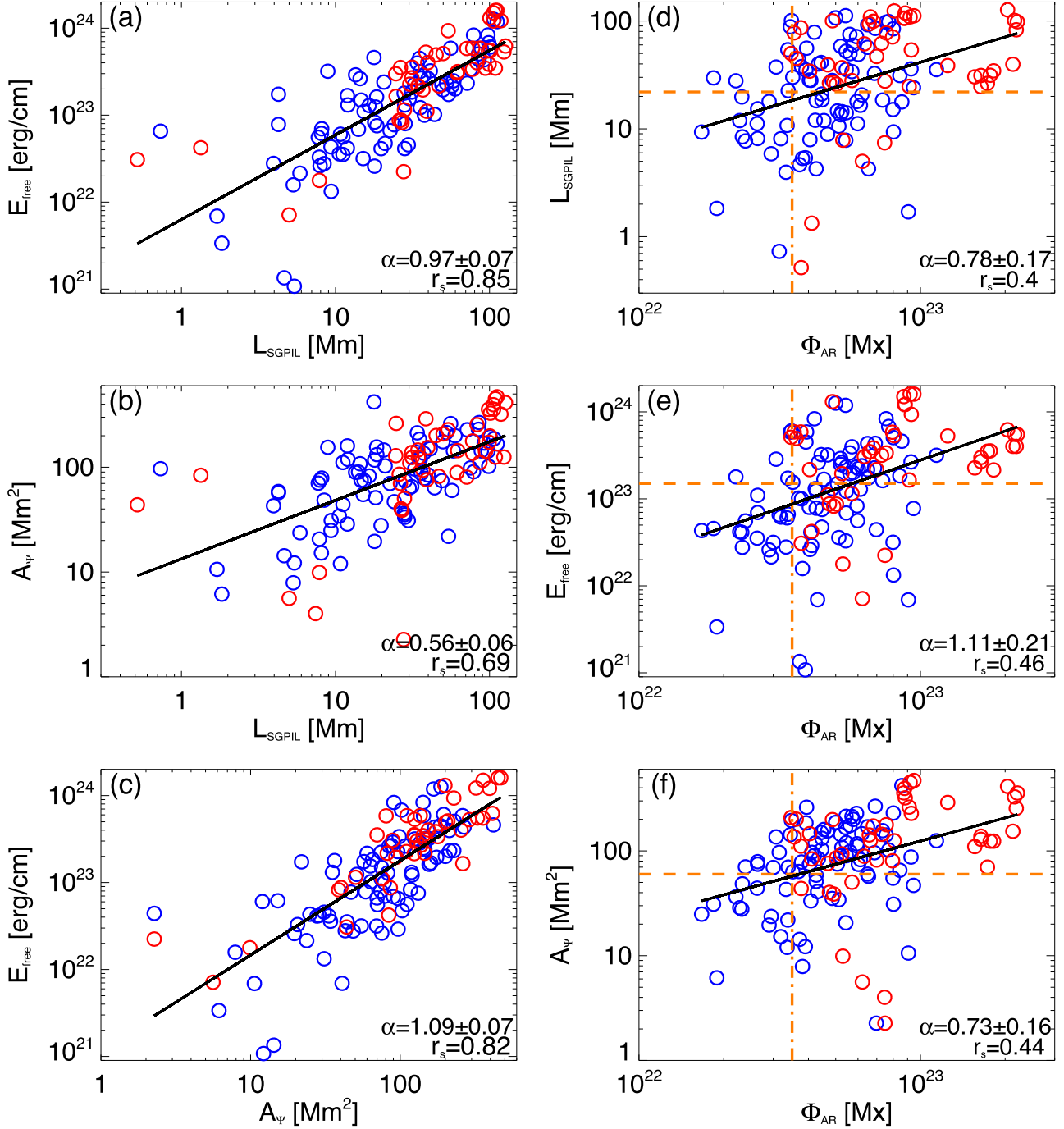


Figure 4. Relations between L_{SGPIL} , E_{free} , A_{ψ} , and Φ_{AR} for eruptive (blue) and confined (red) flares. The black solid lines show the results of a linear fitting, and slopes α and Spearman rank order correlation coefficients r_s are shown at the bottom right of each panel. Orange dashed-dotted lines in panels (d)–(f) correspond to Φ_{AR} of 3.5×10^{22} Mx. Orange dashed lines denote L_{SGPIL} of 22 Mm, E_{free} of 1.5×10^{23} erg cm^{-1} , and A_{ψ} of 60 Mm^2 .

are eruptive. However, for the remanent 85 flares with $L_{\text{SGPIL}} > 22$ Mm, it is difficult to tell whether or not a flare is accompanied by a CME. The appearance of the other two parameters is similar to that of L_{SGPIL} . Only a fraction of flare events can be discriminated between confined and eruptive events. Thus we speculate that if we use these “extensive” parameters to predict the CME productivity, the True Skill Score (TSS) value is not high. This is consistent with the study of Bobra & Ilonidis (2016), who shows that TSS for predicting the CME productivity is low based on “extensive” parameters.

They show that “intensive” parameters can predict the CME productivity. In our study, we did not calculate “intensive” parameters. In our future work, we will consider “intensive” parameters in confined and eruptive large flares based on our database.

In the statistical results of Cui et al. (2018), confined flares have larger values of Φ_{AR} and the gradient-weighted area of the polarity-inversion region than eruptive flares, which are in agreement with our results. It was found that large confined flares tend to occur in large ARs (Toriumi et al. 2017; Li et al.

2020), and thus L_{SGPIL} , E_{free} , and A_{Ψ} are larger for confined than eruptive flares due to their positive correlations with Φ_{AR} . Our results imply that Φ_{AR} is a key factor in determining whether a flare is eruptive or confined, as it provides a global parameter relating to the strength of the background field confinement.

This work is supported by the National Key R&D Program of China (2019YFA0405000), the B-type Strategic Priority Program of the Chinese Academy of Sciences (XDB41000000), the National Natural Science Foundation of China (11773039, 11903050, 12073001, 11790304, 11873059, and 11790300), Key Programs of the Chinese Academy of Sciences (QYZDJ-SSW-SLH050), the Youth Innovation Promotion Association of CAS (2014043 and 2017078), Yunnan Academician Workstation of Wang Jingxiu (No. 202005AF150025) and NAOC Nebula Talents Program. A. Q.C. is supported by the Strategic Priority Program on Space Science, Chinese Academy of Sciences, grant No. XDA15350203. A.M.V. acknowledges the support by the Austrian Science Fund (FWF): P27292-N20. SDO is a mission of NASA's Living With a Star Program.

ORCID iDs

Ting Li  <https://orcid.org/0000-0001-6655-1743>
 Anqin Chen  <https://orcid.org/0000-0002-3325-7385>
 Yijun Hou  <https://orcid.org/0000-0002-9534-1638>
 Astrid M. Veronig  <https://orcid.org/0000-0003-2073-002X>
 Shuhong Yang  <https://orcid.org/0000-0002-6565-3251>

References

Andrews, M. D. 2003, *SoPh*, **218**, 261
 Argiroffi, C., Reale, F., Drake, J. J., et al. 2019, *NatAs*, **3**, 742
 Baumgartner, C., Thalmann, J. K., & Veronig, A. M. 2018, *ApJ*, **853**, 105
 Bobra, M. G., & Ilonidis, S. 2016, *ApJ*, **821**, 127
 Bobra, M. G., Sun, X., Hoeksema, J. T., et al. 2014, *SoPh*, **289**, 3549
 Brueckner, G. E., Howard, R. A., Koomen, M. J., et al. 1995, *SoPh*, **162**, 357

Chen, A., & Wang, J. 2020, *SCPMA*, **63**, 269512
 Chen, A. Q., & Wang, J. X. 2012, *A&A*, **543**, A49
 Cui, Y., Wang, H., Xu, Y., et al. 2018, *JGRA*, **123**, 1704
 DeRosa, M. L., & Barnes, G. 2018, *ApJ*, **861**, 131
 Drake, J. J., Cohen, O., Yashiro, S., et al. 2013, *ApJ*, **764**, 170
 Duan, A., Jiang, C., He, W., et al. 2019, *ApJ*, **884**, 73
 Falconer, D. A., Moore, R. L., & Gary, G. A. 2002, *ApJ*, **569**, 1016
 Gupta, M., Thalmann, J. K., & Veronig, A. M. 2021, arXiv:2106.08781
 Howard, R. A., Moses, J. D., Vourlidas, A., et al. 2008, *SSRv*, **136**, 67
 Jing, J., Liu, C., Lee, J., et al. 2018, *ApJ*, **864**, 138
 Jing, J., Tan, C., Yuan, Y., et al. 2010, *ApJ*, **713**, 440
 Kaiser, M. L., Kucera, T. A., Davila, J. M., et al. 2008, *SSRv*, **136**, 5
 Kazachenko, M. D., Lynch, B. J., Welsch, B. T., et al. 2017, *ApJ*, **845**, 49
 Kontogiannis, I., Georgoulis, M. K., Guerra, J. A., et al. 2019, *SoPh*, **294**, 130
 Leitzinger, M., Odert, P., Greimel, R., et al. 2014, *MNRAS*, **443**, 898
 Lemen, J. R., Title, A. M., Akin, D. J., et al. 2012, *SoPh*, **275**, 17
 Li, T., Hou, Y., Yang, S., et al. 2020, *ApJ*, **900**, 128
 Liu, L., Wang, Y., Wang, J., et al. 2016, *ApJ*, **826**, 119
 Machara, H., Shibayama, T., Notsu, S., et al. 2012, *Natur*, **485**, 478
 Mayfield, E. B., & Lawrence, J. K. 1985, *SoPh*, **96**, 293
 Molodensky, M. M. 1974, *SoPh*, **39**, 393
 Moore, R. L., Sterling, A. C., Hudson, H. S., et al. 2001, *ApJ*, **552**, 833
 Moschou, S.-P., Drake, J. J., Cohen, O., et al. 2019, *ApJ*, **877**, 105
 Nindos, A., & Andrews, M. D. 2004, *ApJL*, **616**, L175
 Odert, P., Leitzinger, M., Hanslmeier, A., et al. 2017, *MNRAS*, **472**, 876
 Pesnell, W. D., Thompson, B. J., & Chamberlin, P. C. 2012, *SoPh*, **275**, 3
 Scherrer, P. H., Schou, J., Bush, R. I., et al. 2012, *SoPh*, **275**, 207
 Schrijver, C. J. 2007, *ApJL*, **655**, L117
 Shibata, K., Isobe, H., Hillier, A., et al. 2013, *PASJ*, **65**, 49
 Su, J. T., Jing, J., Wang, S., et al. 2014, *ApJ*, **788**, 150
 Sun, X., Bobra, M. G., Hoeksema, J. T., et al. 2015, *ApJL*, **804**, L28
 Thalmann, J. K., Su, Y., Temmer, M., et al. 2015, *ApJL*, **801**, L23
 Toriumi, S., Schrijver, C. J., Harra, L. K., et al. 2017, *ApJ*, **834**, 56
 Toriumi, S., & Wang, H. 2019, *LRSP*, **16**, 3
 Vasantharaju, N., Vemareddy, P., Ravindra, B., et al. 2018, *ApJ*, **860**, 58
 Veronig, A. M., Odert, P., Leitzinger, M., et al. 2021, *NatAs*, **5**, 697
 Vida, K., Leitzinger, M., Kriskovics, L., et al. 2019, *A&A*, **623**, A49
 Wang, H., Ewell, M. W., Zirin, H., et al. 1994, *ApJ*, **424**, 436
 Wang, J., Shi, Z., Wang, H., et al. 1996, *ApJ*, **456**, 861
 Wang, J., Zhang, Y., Hess Webber, S. A., et al. 2020, *ApJ*, **892**, 140
 Wang, Y., & Zhang, J. 2007, *ApJ*, **665**, 1428
 Yang, S., Zhang, J., & Xiang, Y. 2014, *ApJL*, **793**, L28
 Yashiro, S., Akiyama, S., Gopalswamy, N., et al. 2006, *ApJL*, **650**, L143
 Zhang, J., Li, L., & Song, Q. 2007, *ApJL*, **662**, L35